# Numerical Study on Fan Spray for Gasoline Direct Injection Engines

Shirabe, Naotaka
R&D Dept. NIPPON SOKEN, INC. : General Maneger

Sato, Takaaki
R&D Dept. NIPPON SOKEN, INC.

Murase, Eiichi
Department of Mechanical Engineering Science : Professor



出版情報：九州大学工学紀要. 63 (1), pp.1-21, 2003-03-26. 九州大学大学院工学研究院
バージョン：
権利関係：

Memoirs of the Faculty of Engineering, Kyushu University, Vol. 63, No. 1, March 2003

# Numerical Study on Fan Spray for Gasoline Direct Injection Engines

by

Naotaka SHIRABE*, Takaaki SATO** and Eiichi MURASE***

(Received November 29, 2002)


## Abstract

In gasoline direct injection engines, it is important to optimize fuel spray characteristics, which strongly affect stratified combustion process. Spray simulation is expected as a tool for optimizing the nozzle design. Conventional simulation method, however, cannot predict the effect of various nozzle geometries on the spray characteristics, because they are based on the experimental data and/or the empirical laws regarding spray boundary condition at the nozzle exit. In Japan, a fan spray injected from a slit type nozzle has been adopted recently for gasoline direct injection engines. This paper proposes a computational model for the fan spray. The structure of two-phase flow inside the nozzle was numerically analyzed using the volume of fluid (VOF) method in a three-dimensional CFD code based on the nozzle geometry. Then, applying the results of these analyses to the linear instability theory, the mean diameter of fuel droplets at the nozzle exit was calculated. These results leaded to the boundary condition at the nozzle exit for the spray simulation instead of the experimental data and/or the empirical laws. Then, the discrete droplet model (DDM) and many sub-models were used for the spray calculation. Spray tip penetration, Sauter mean diameter (SMD), and spray mass flow rate distribution were verified for various pressures and nozzle geometries.


**Keywords:** Fan spray, Slit nozzle, Direct injection, Spray simulation, Breakup model, VOF method

## 1. Introduction

From the aspect of environmental protection in recent years, worldwide demands for reductions in fuel consumption and $CO_2$ emission in gasoline engines have been made. Gasoline direct injection engines, which offer a good response to this requirement, have

*General Maneger, R & D Dept. NIPPON SOKEN, INC.
**R & D Dept. NIPPON SOKEN, INC.
***Professor, Department of Mechanical Engineering Science

already been in mass production. In gasoline direct injection engines, fuel consumption is reduced by stratified combustion under partial load. To maintain stable stratified combustion in gasoline direct injection engines, fuel and gas mixture formation in the cylinder must be precisely controlled. Therefore, the fuel injector requirements are becoming hard to meet. The swirl injector, which injects hollow-cone spray and is most popular for gasoline direct injection engines, is used by Mitsubishi[1], Toyota[2)3)] and so on. In contrast, Toyota has recently introduced a new slit-type injector, which injects fan spray to improve engine performance[4)5)6)17)]. As the fan spray has longer penetration length than hollow-cone spray, charge motion, such as a swirl flow, is not essential in creating a combustible mixture around the spark plug, if an appropriately shaped piston is used. A straight port, which has high trapping efficiency, can therefore be used instead of a helical port.

Spray simulation is expected to be a useful tool in designing the nozzles of injectors. In the conventional spray simulation, the fuel breakup process is divided into two parts: "primary breakup", in which a liquid column or sheet injected from the nozzle exit disintegrates into droplets; "secondary breakup", in which a droplet breaks into smaller droplets. In the conventional simulation, the discrete droplet model (DDM)[7] is used for calculating secondary breakup, droplet motion, breakup, and evaporation. In DDM, the droplet size distribution and the velocity after primary breakup are required as boundary conditions at the nozzle exit. However, there is no adequate primary breakup model anywhere in the world. Therefore in conventional way, DDM boundary conditions at the nozzle exit are derived experimentally or empirically. In this method, the experiment with each nozzle geometry is required to decide the boundary conditions at the nozzle exit. The spray characteristics of a new nozzle therefore cannot be predicted without an experiment using the nozzle itself. Therefore, this model cannot be used for the nozzle design. To improve this problem, several models have been proposed for swirl injectors. Ren and Nally[8] calculated the fuel flow inside the nozzle with three-dimensional CFD. The output of this calculation and the wave instability theory were used to calculate the droplet mean diameter after primary breakup. The results were used for the initial data of the spray simulation. In this model, the nozzle geometric parameters can directly affect the calculated spray characteristics. Xu and Markle[9] proposed a similar approach for the outwardly opened swirl injector. Arcoumanis et al.[10] used the two-dimensional two-phase flow model to calculate the fuel flow inside the nozzle more accurately.

This paper proposes an advanced model for the fan spray injected from a slit injector employing the fully two-phase three-dimensional flow model to calculate the flow inside the nozzle using the linear instability theory and the droplet size distribution.

## 2. Experimental Analysis

Before developing the simulation model, the slit-injected fan spray was observed in detail. **Figure 1** shows the experimental apparatus. Spray shadow graphs were obtained using the CCD camera and the pulse light synchronized with the fuel injection system. **Figure 2** shows the shape of the prototyped slit nozzle. **Table 1** shows the observation conditions. The width of the view was 2 - 6 mm below the nozzle exit. **Figure 3** shows the observed result. The fuel emitted from the nozzle hole formed a liquid film. A wave gradually appeared on the film surface. The wavelength was about 0.37 mm. Below the wave, the film disintegrated with ligaments, which disintegrated into droplets. In this experiment, in order to visualize the breakup process clearly, the injection pressure (0.5 MPa-abs) was lower than that used in real engines. At the high pressure of around 10 MPa, which is used in real

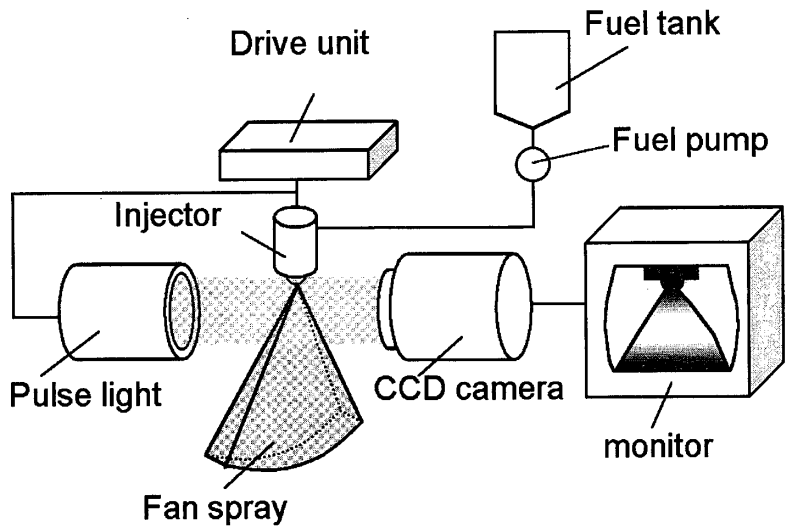


**Fig. 1** Experimental apparatus

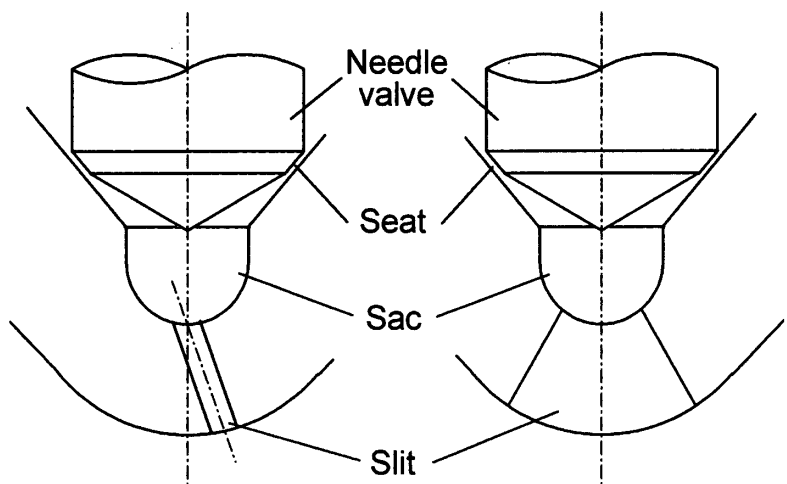


**Fig. 2** Slit nozzle

**Table 1** Experimental conditions

| Fuel | n-heptane |
|---|---|
| Injection pressure | 0.5MPa-abs |
| Injection pulse | 3.0ms |
| Photographing timing | 2.0ms after injection start |
| Ambient pressure | 101kPa-abs |
| Ambient temperature | 293K |

engines, we could not observe the breakup process clearly. In this paper, we assume that the breakup process is the same at both low and high pressures, but we have to ensure this assumption. On the above assumption, the breakup regime was compared with breakup theory as concerns liquid film. **Figure 4** shows the breakup theory presented by Fraser et al.[11)12)]. In this theory, the wavelength is shown in Eq. (1), and it appears that its amplitude increases gradually until the disintegration occurs.

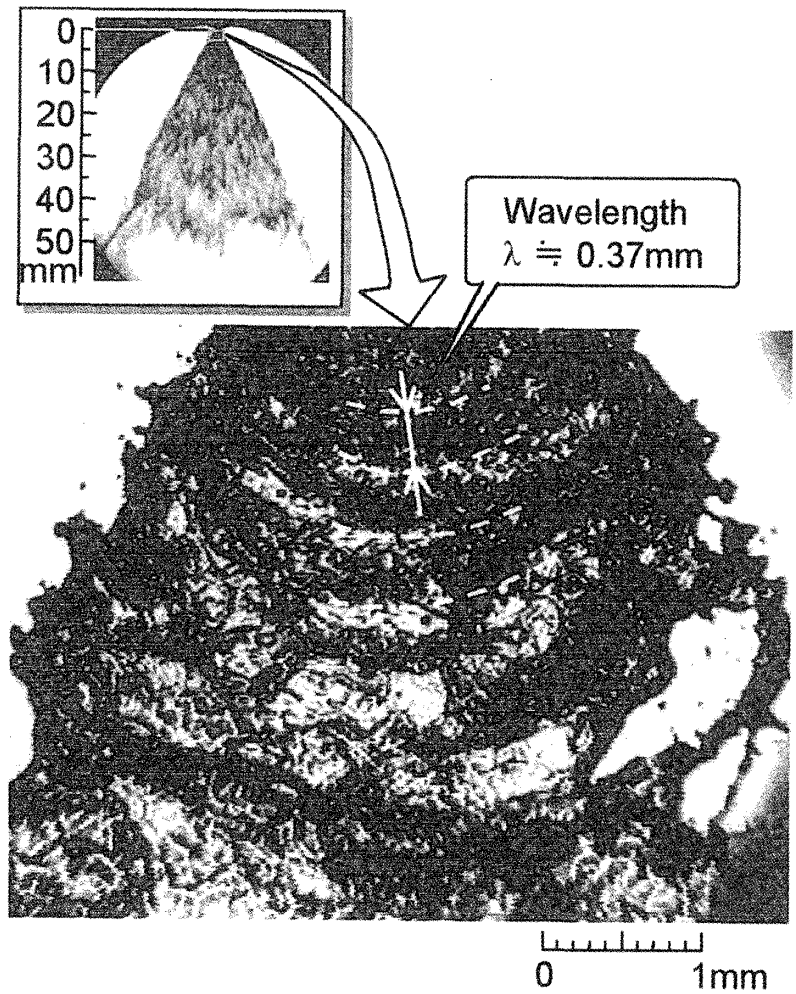


**Fig. 3** Observation result

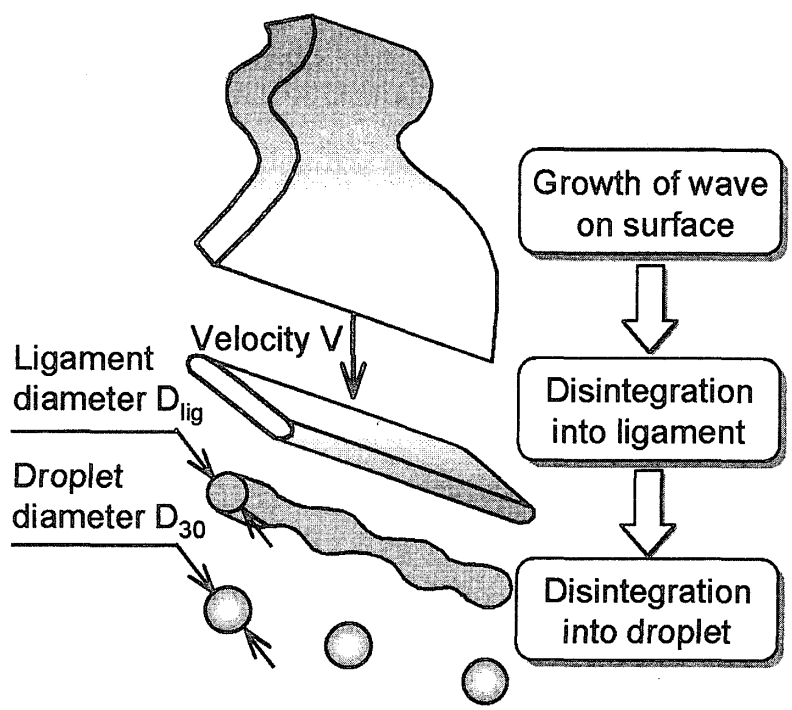


**Fig. 4** Schema of classical breakup theory presented by R. P. Fraser, et al.

$$\lambda_{opt}=\frac{4\pi\sigma}{\rho_a \cdot V^2} \tag{1}$$

Here, $\lambda_{opt}$, $\sigma$, $\rho_a$, and $V$ represent the wavelength appearing on the liquid sheet surface, surface tension force, ambient gas density, and liquid sheet velocity, respectively. The features of this breakup regime are very similar to those of the observed fan spray.

The wavelength calculated by the breakup theory is compared with the observed result. The wave velocity measured by high speed camera is 24.3 m/s; $\sigma$ and $\rho_a$ are $19.8\text{x}10^{-3}$ N/m and 1.184 kg/m$^3$, respectively. So the calculated wavelength by Eq. (1) becomes 0.36 mm, and it is nearly equal to the observed value of 0.37 mm. It is therefore concluded that the breakup regime of the fan spray injected from the slit injector for gasoline direct injection engines can be calculated based on the breakup theory presented by Fraser et al.

## 3. Computational Models

On the basis of the above result, the breakup theory[11)12)] is used as the primary breakup model for the fan spray simulation. In the breakup theory, volume mean diameter $D_{30}$ is calculated using Eq. (5) which is derived from Eqs. (1), (2), (3), and (4).

$$\frac{\lambda_{opt} \cdot h^*}{2}=\frac{\pi}{4}D_{lig}{}^2 \tag{2}$$

$$D_{30}=1.89D_{lig} \tag{3}$$

$$h^*=\left(\frac{1}{2E^2}\right)^{\frac{1}{3}}\left(h^2 r^2 \frac{\rho_a V^2}{\rho_L \sigma}\right)^{\frac{1}{3}} \tag{4}$$

$$D_{30}=3.78\left(\frac{2}{E}\right)^{\frac{1}{3}}\left(\frac{hr}{V^2}\right)^{\frac{1}{3}}\left(\frac{\sigma^2}{\rho_L \rho_a}\right)^{\frac{1}{6}} \tag{5}$$

Here, $h^*$, $D_{lig}$, $E$, $h$, $\rho_L$ are liquid film thickness at the breakup point, ligament diameter, experimental constant, liquid film thickness at radial distance $r$, and liquid density, respectively. The left term of Eq. (2) shows the section area of half wavelength of the liquid sheet at the breakup point, while the right term shows the ligament section area. Equation (3) is derived from Rayleigh's analysis, and Eq. (4) is from the experiments and the analysis carried out at various densities and liquid velocities by Fraser et al.[12)]. In Eq. (5), liquid thickness $h$ at radial distance $r$ and liquid film velocity $V$ are required to calculate $D_{30}$. The three-dimensional CFD inside the nozzle is used to derive these variables, but the conventional 3D CFD model cannot calculate the liquid thickness accurately, because it cannot take both liquid and gas phase into account simultaneously. It takes only the liquid phase. In this paper, therefore, the two-phase 3D CFD is employed. Recently, some 3D CFD models have been advocated. Here, the Volume of Fraction (VOF) model[13)] is used because it is installed in the commercial CFD code Star-CD. In the VOF model, liquid ratio $F$ in each cell is derived using Eq. (6).

$$\frac{\partial F}{\partial t}+u\frac{\partial F}{\partial x}+v\frac{\partial F}{\partial y}+w\frac{\partial F}{\partial z}=0 \tag{6}$$

Using Eq. (6) together with the equation of the continuity and N. S. equation, liquid thickness $h$ at the nozzle exit and the liquid film velocity $V$ can be calculated accurately, as long as the cavitation inside the nozzle does not take place. The use of this result with the breakup theory yields volume mean diameter $D_{30}$, which takes the nozzle design parameter into account.

It seems appropriate to assume that there are various size of droplets after the primary breakup while the droplet size after the primary breakup calculated from the above model

is only the mean value. So in this paper, droplet size distributions in each spray direction are determined using the Nukiyama-Tanasawa distribution function as described in Eq. (7), and the volume mean

$$\phi = aD^p \cdot \exp[-(bD)^q] \tag{7}$$

$$Q = \frac{4}{3}\pi \int D^3 \phi dD \tag{8}$$

$$D_{30} \equiv \left( \frac{\int D^3 \phi dD}{\int \phi dD} \right)^{\frac{1}{3}} \tag{9}$$

diameter $D_{30}$ can be calculated as above. Here, $a$, $b$, $p$ and $q$ are the constants derived from Eqs. (8) and (9) in each direction. The volume mean diameter $D_{30}$ and the mass flow rate $Q$ derived above are used here.

Using the model described above, the distribution of the liquid sheet thickness and the velocity can be calculated from the nozzle design parameters and conditions. The use of the breakup theory and the Nukiyama-Tanasawa distribution function with these variables enables the determination of post-primary breakup droplet size distribution without actual experiment. So, we can calculate the spray characteristics of a new nozzle by using only its design parameters and conditions. Therefore this model is able to be used for the nozzle design.

## 4. Results and Discussions

### 4.1 Two-phase 3D CFD inside nozzle and droplet size distribution after primary breakup

Two-phase three-dimensional CFD was carried out on the interior of the prototyped nozzle A for gasoline direct injection engines. **Figure 5** shows the shape of the nozzle A. The sac diameter and the slit thickness are 0.8 mm and 0.16 mm, respectively. The slit axis crosses the injector axis at the sac bottom. **Figure 6** shows the computational domain and the mesh of the nozzle A. The computational domain was only half the nozzle because its shape was symmetrical. The "balloon" was placed below the slit to solve stable and accurately. **Table 2** shows the Nozzle internal flow calculation conditions. The code used

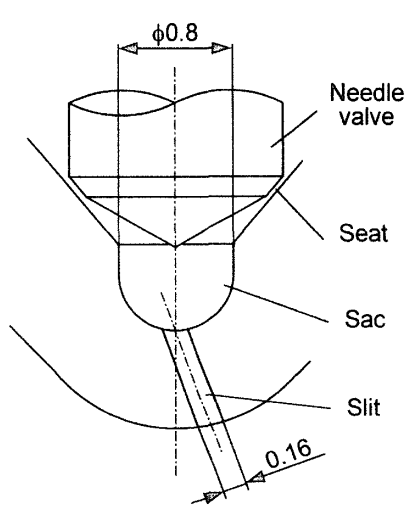


**Fig. 5** Nozzle A

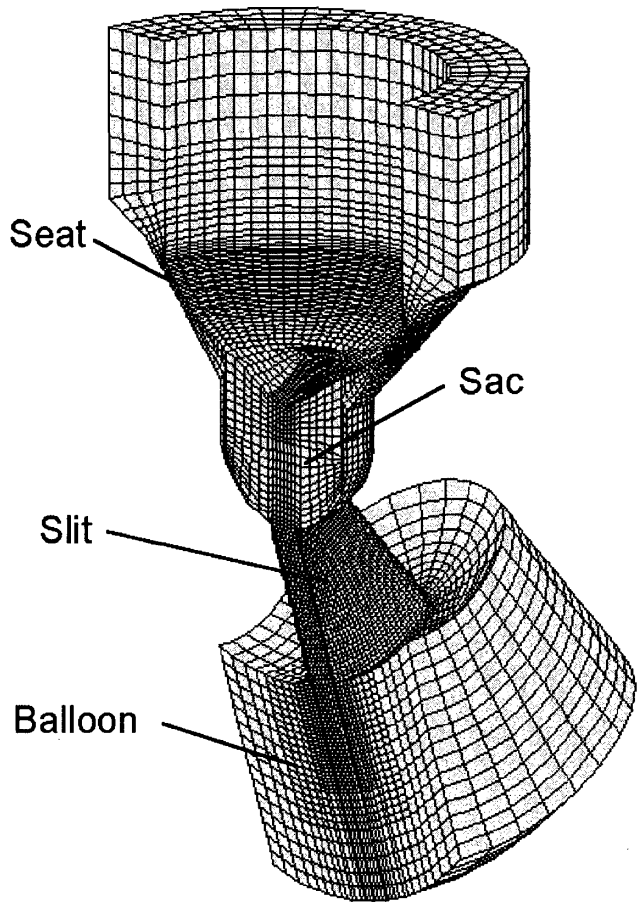


**Fig. 6** Computational domain and mesh

**Table 2** Nozzle internal flow calculation conditions

| CFD code | STAR-CD |
|---|---|
| Fuel | n-heptane |
| Injection pressure | 11MPa-abs |
| Ambient pressure | 280kPa-abs |
| Needle lift | 50μm |
| Turbulence model | Standard k-ε |

was "Star-CD", which supports the VOF model. The ambient pressure was set at 280 kPa-abs, as the ambient gas density corresponding to that inside the engine cylinder at the time of injection.

**Figure 7** shows the results of the two-phase 3D CFD for the nozzle A at 1.0 ms after the start of injection. The gray area represents the liquid phase, while the white area represents the gas phase. The boundary between liquid and gas is clearly delineated, revealing that the liquid sheet thickness at the nozzle exit is thinner than the slit thickness, and its distribution with $\theta$ is not uniform. The time-averaged thickness from 0.6ms to 1.0 ms after the start of calculation was used here, because it fluctuated a little. **Figure** 8 shows the liquid sheet thickness $h$ distribution with $\theta$. The thickness $h$ is greater at both center and side of the slit. **Figure 9** shows the liquid sheet velocity $V$ distribution at the nozzle exit. It is also the

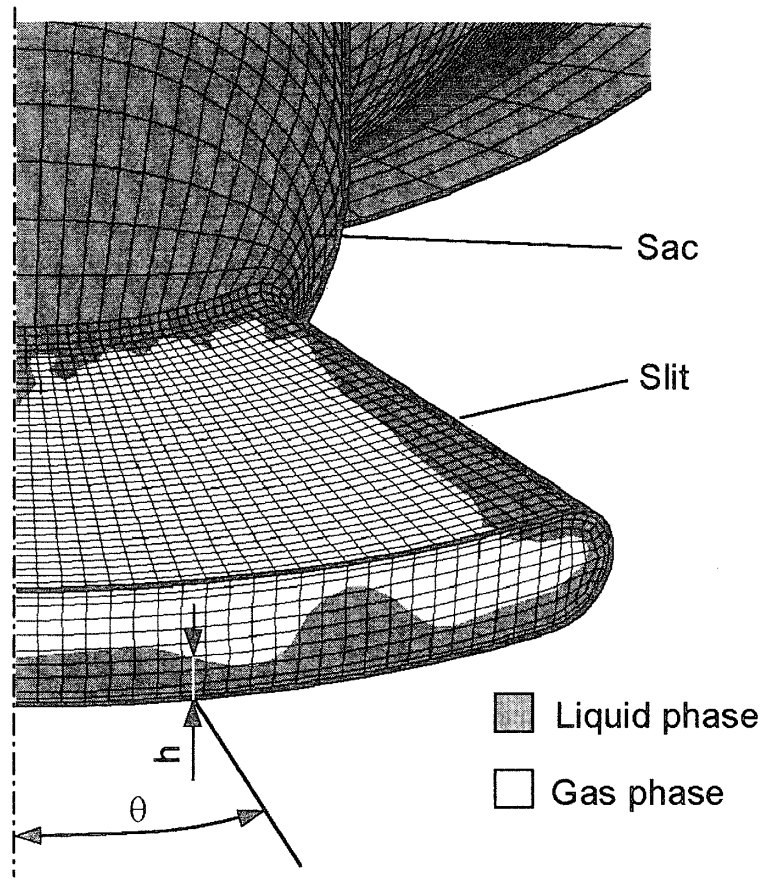


**Fig. 7** Nozzle internal flow calculation result

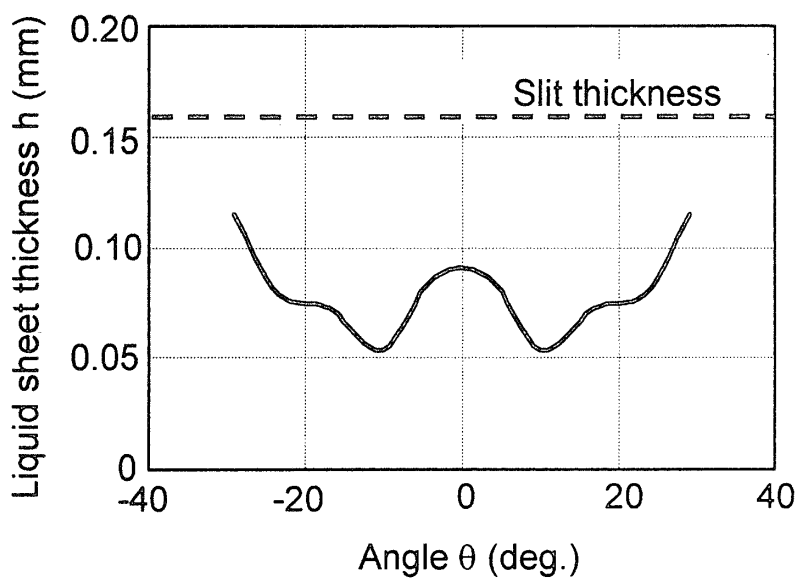


**Fig. 8** Liquid sheet thickness distribution at nozzle exit

averaged value from 0.6 ms to 1.0 ms after the start of calculation, because of its fluctuation. From these variables, mass flow rate ($=h\times V$) and volume mean diameter $D_{30}$ after the primary breakup were calculated with each direction $\theta$ using the breakup theory. **Figure 10** shows the volume mean diameter $D_{30}$ distribution after the primary breakup for the nozzle A. The distribution is similar to the liquid thickness distribution as shown in **Fig. 8**.

**Figure 11** shows the result of the droplet size distribution after the primary breakup with

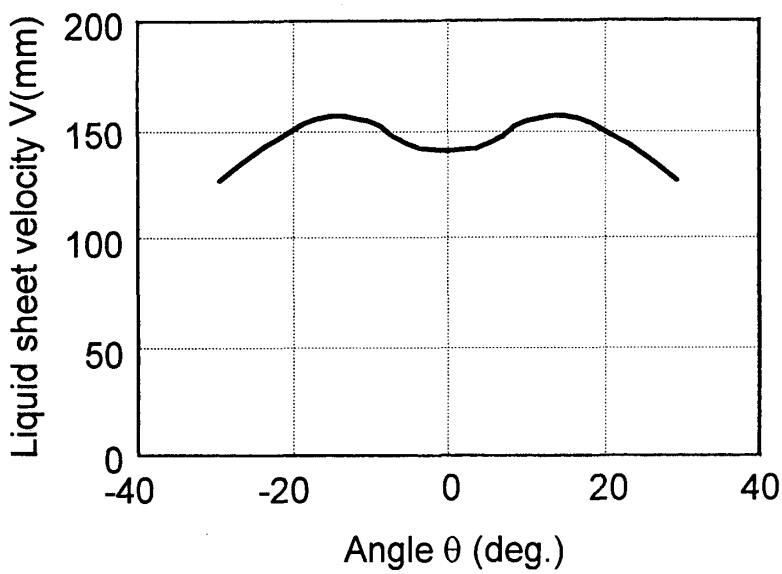


**Fig. 9** Liquid sheet velocity distribution at nozzle exit

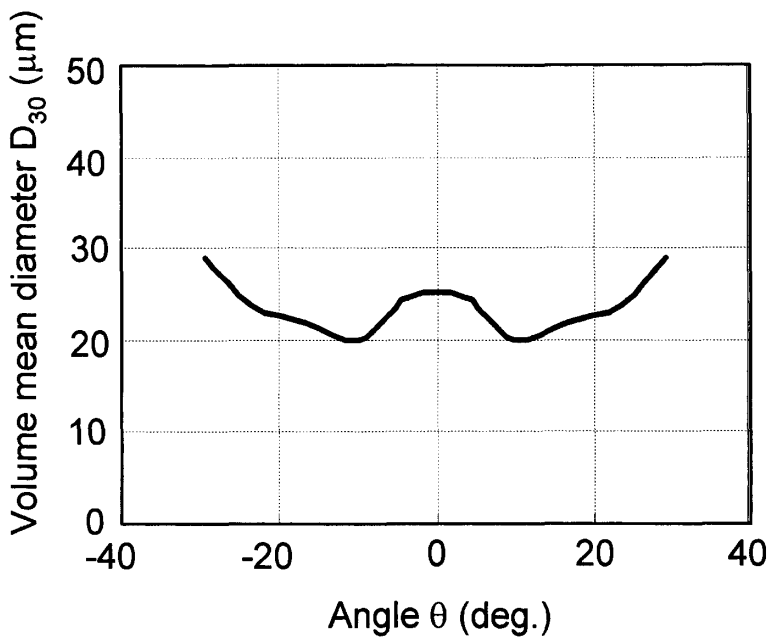


**Fig.10** Volume mean droplet diameter distribution after primary breakup

each direction $\theta$. Distribution was obtained using the Tanasawa-Nukiyama distribution function with constants derived from the mass flow rate and the volume mean diameter calculated by the breakup theory as described above.

### 4.2 Spray simulation

The liquid velocity and the droplet size distribution calculated above were used as the input data of the spray simulation for the nozzle A. **Table 3** shows the spray conditions of the simulation and the experiment. The computer code used was FIRE, which had many spray sub-models. In this paper, WAVE[14)15)] was used for secondary breakup model. Collision and Evaporation are also taken into account. **Figure 12** depicts the calculated and the measured spray images for the nozzle A at 1.2 ms after the start of injection. In the calculation, a vertical line was appeared due to the mesh influence. But it had little influence on the spray characteristics, such as the mass flow rate distribution and SMD (Sauter mean

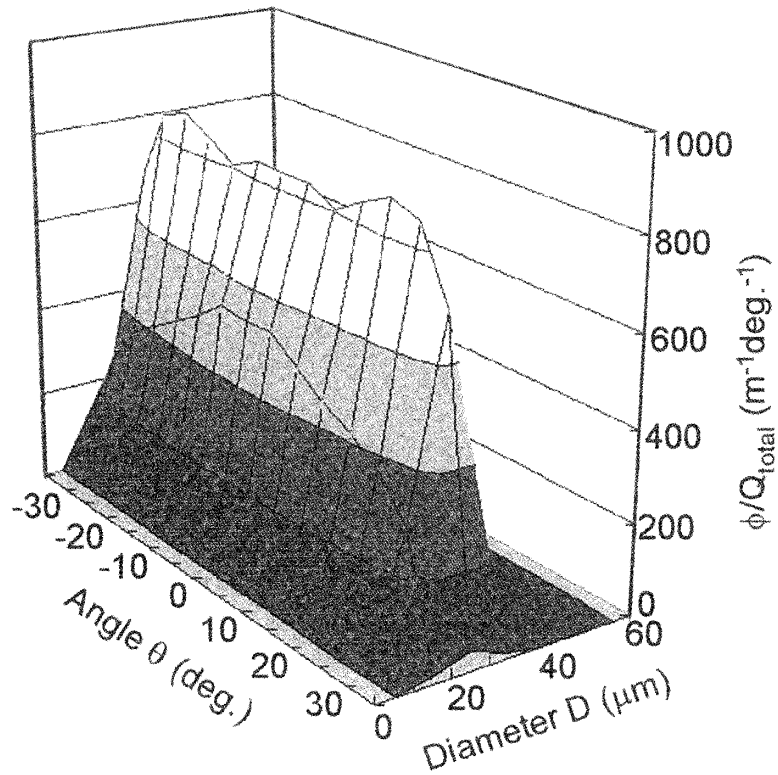


**Fig.11** Droplet size distribution after primary breakup

**Table 3** Spray calculation conditions

| CFD code | FIRE |
|---|---|
| Fuel | n-heptane |
| Injection pressure | 11MPa-abs |
| Ambient pressure | 280kPa-abs |
| Injection quantity | 13.6$mm^3$/st |
| Turbulence model | Standard k-ε |
| Ambient temperature | 293K |

diameter) distribution which can be seen in **Figs. 14** and **17**. Due to the time variation, the side penetration of the spray of the measured image was longer than that of the computational image. The dotted line in **Fig. 12** shows the averaged tip shape for 10 measurements. This line shows good agreement with the computational tip shape image. **Figure 13** depicts the calculated and the measured spray tip penetration for the nozzle A. The spray tip penetration was defined as the vertical length of the portion of the intensity higher than the threshold in the spray image averaged for 10 injections. In the calculation, the spray tip penetration is also defined as the vertical length of the portion with mass rate 99% of the entire spray. As shown in **Fig. 13**, the gradient of the increase of the spray penetration become high during 0.2 - 0.5 ms, and after 0.5 ms it increased gradually. Good agreement was seen between calculated and experimental values. The developed model can therefore accurately predict the spray image and the tip penetration.

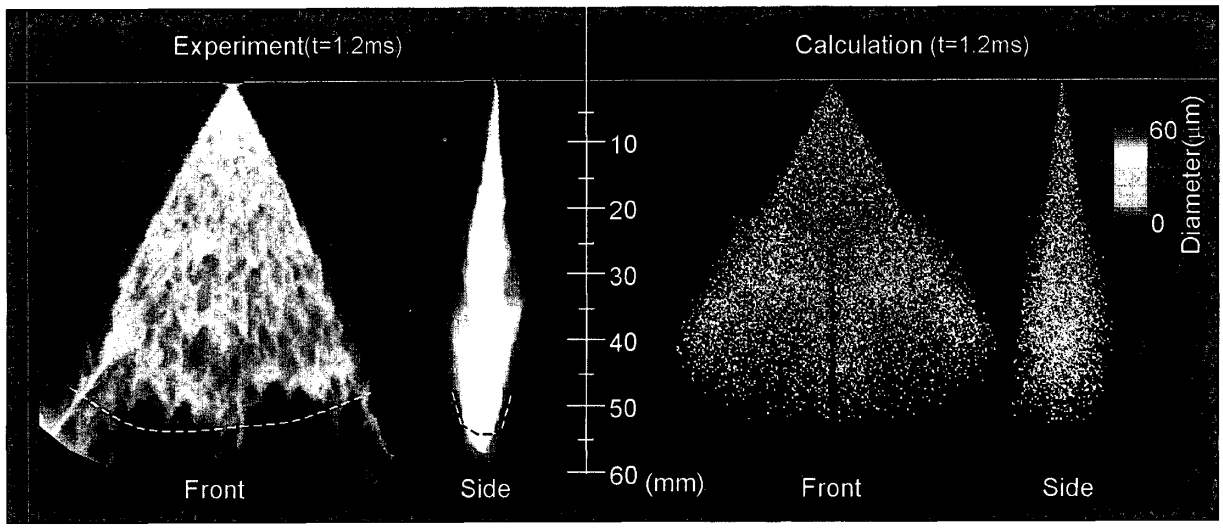


**Fig.12** Comparison of spray image for nozzle A (Pa=280 kPa-abs)

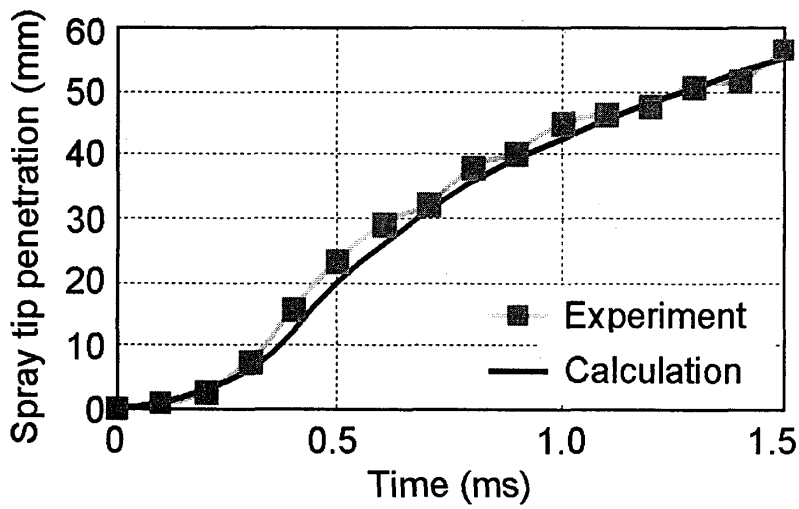


**Fig.13** Spray tip penetration

### 4.3 Verification of mass flow rate and SMD distribution inside spray

Mass flow rate and SMD distribution inside the spray were verified for the case described above. **Figure 14** depicts the calculated and the measured mass flow rate distribution for the nozzle A. In the experiment, receptacles 7 mm wide were arranged 55 mm below the nozzle exit; after 500 injections, the fuel mass in the receptacles was measured. As shown in **Fig. 14**, the feature of uniformity of the mass distribution with spray angle is simulated accurately.

The droplet diameter inside the spray was measured using laser holography which enables the droplet diameter measurement at any part of the spray after taking the holograph, because all droplet shapes are recorded as 3D images on a holographic plate. **Figures 15** and **16** show the experimental apparatus. Interference fringes, which were generated by interfering between object beam and reference beam, were recorded on the holographic plate. The spray image was reconstructed by irradiating the plate with a reconstruction beam. The 3D moving stage provided automatic measurement at reconstruction. **Figure 17** depicts the calculated and the measured SMD distribution for the nozzle A at 40 mm below the nozzle exit, 1.2 ms after the start of injection. The examined volume was 1 mm×1.5 mm×0.3 mm in the experiment, while it was 5 mm×4 mm×50 mm (depth) in the calculation. As shown

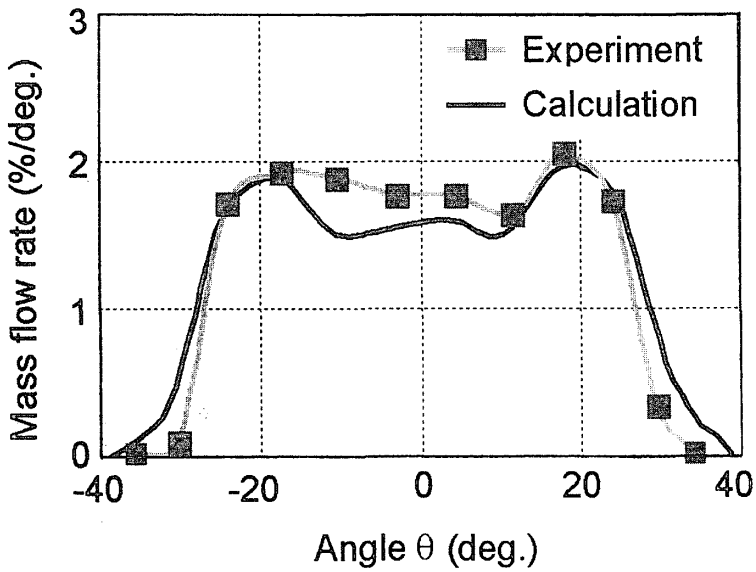


**Fig.14** Mass flow rate distribution for nozzle A

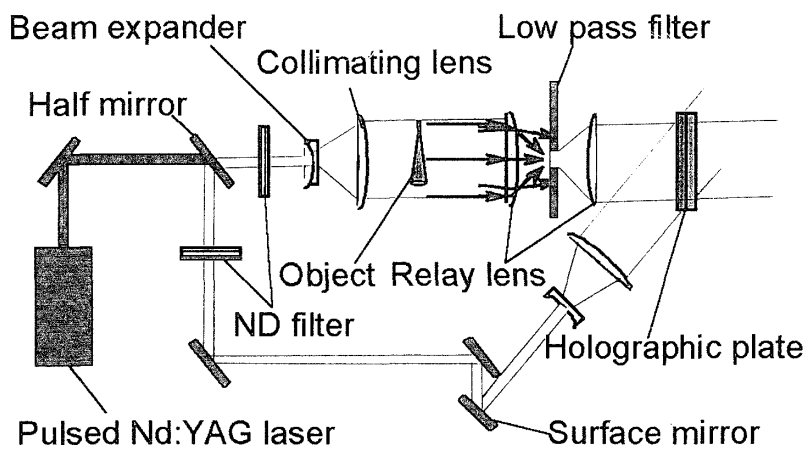


**Fig.15** Optical system used in recording holograms

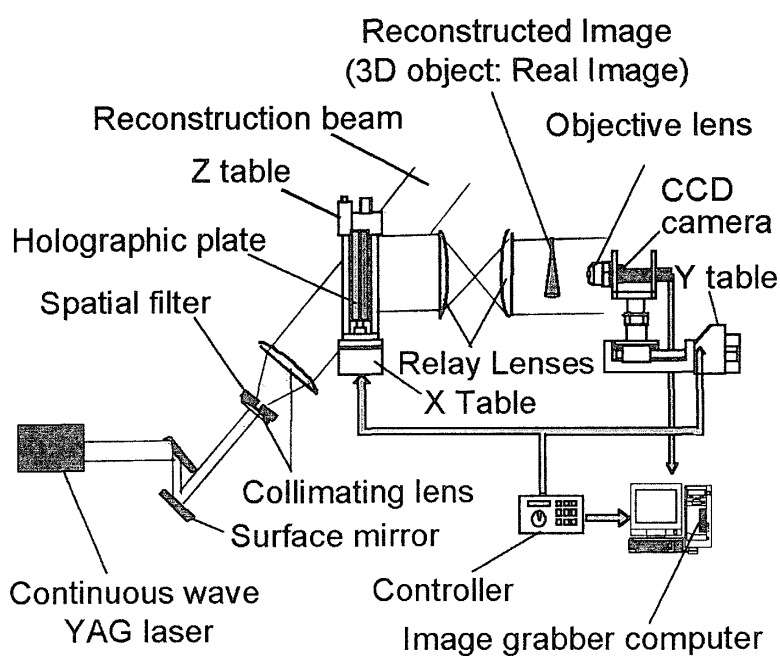


**Fig.16** Optical system used in hologram reconstruction

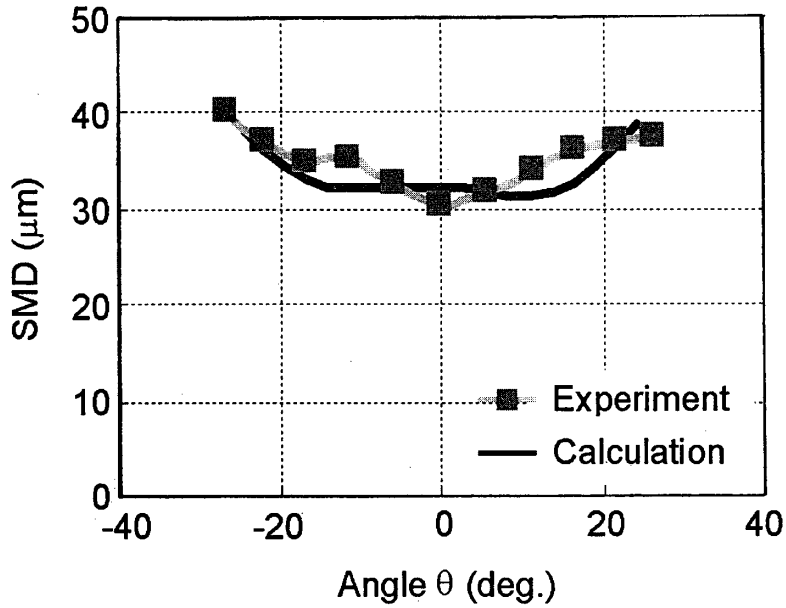


**Fig.17** SMD distribution

in **Fig. 17**, SMD was simulated accurately. Based on the above result, it is concluded that the spray characteristics such as mass distribution and SMD distribution inside the spray can be predicted accurately using this simulation.

### 4.4 Effect of ambient pressure on spray characteristics

The ambient pressure effect on the spray characteristics were examined. Two ambient pressures were chosen; 101 kPa-abs(atmospheric pressure) and 280 kPa-abs. **Figure 18** depicts the calculated and the measured spray images at 101 kPa-abs. The spray image in this case was larger than that in the high ambient pressure case shown in **Fig. 12**. As shown in **Fig.18**, the calculated values show good agreement with the measured one. **Figure 19** shows the calculated and the measured spray tip penetration at 101 kPa-abs and 280 kPa-abs. The calculations also accurately predict the ambient pressure effect. These results confirm

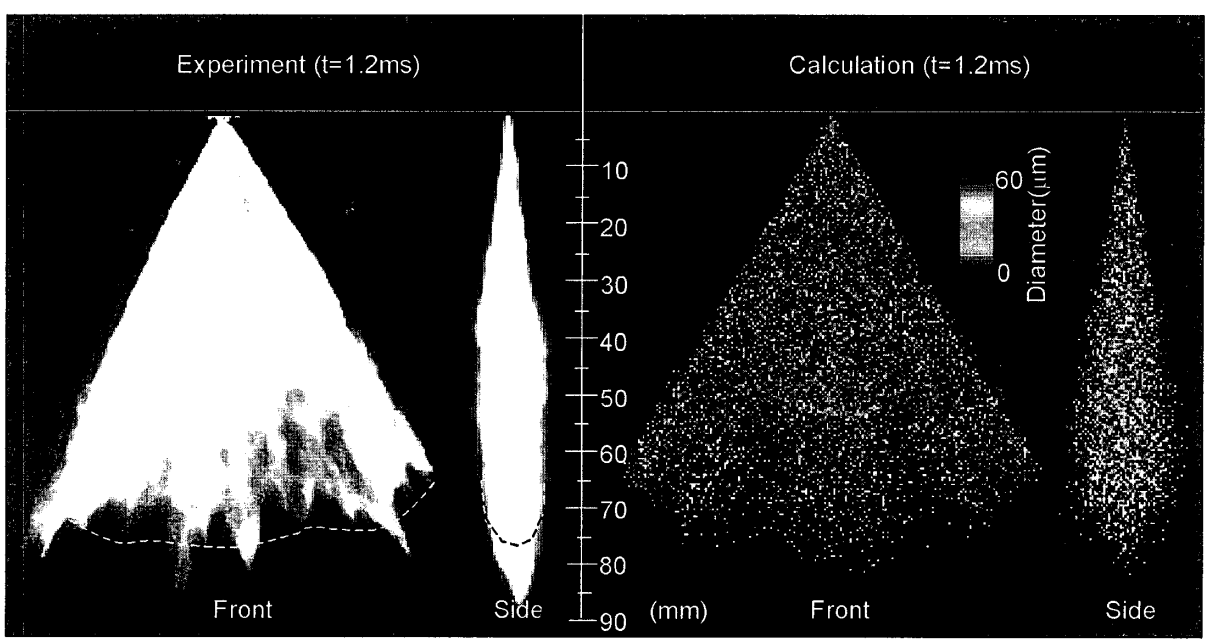


**Fig.18** Comparison of spray image for nozzle A (Pa=101 kPa-abs)

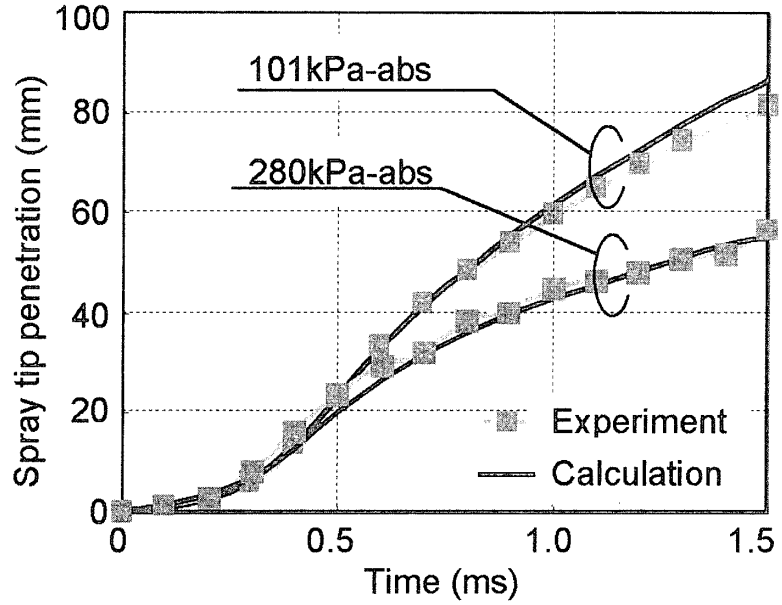


**Fig.19** Spray tip penetration

that the above calculation can accurately estimate the effect of ambient pressure on the spray characteristics.

### 4.5 Effect of nozzle design parameters on spray characteristics

The effect of nozzle design parameters on the spray characteristics was investigated. In addition to the nozzle A, another prototyped nozzle B was used. **Figure 20** shows the shape of the nozzle B whose slit axis was 0.15 mm off to the side and crossing the injector axis at the middle of the sac. The sac diameter and the slit thickness were 1.0 mm and 0.185 mm, respectively. Conditions of the calculation and the experiment are shown in **Table 3**.

**Figure 21** shows the computational and the experimental results for the spray images at 1.2 ms after the start of injection of the nozzle B. The spray tip penetration at the side of the spray of the nozzle B was relatively short and its shape was similar to a teardrop, while that of the nozzle A was long. **Figure 22** shows the mass flow rate distribution inside the spray at 55 mm below the exit of the nozzle B. The mass flow rate distribution of the nozzle B is concentrated at the center, while that of the nozzle A shown in **Fig. 14** is uniform along the spray angle. The calculation can predict these features correctly; therefore, this simulation can predict the effect of the nozzle design parameters on the spray characteristics.

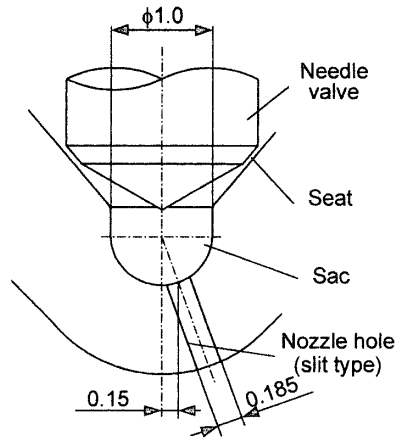


**Fig.20** Nozzle B

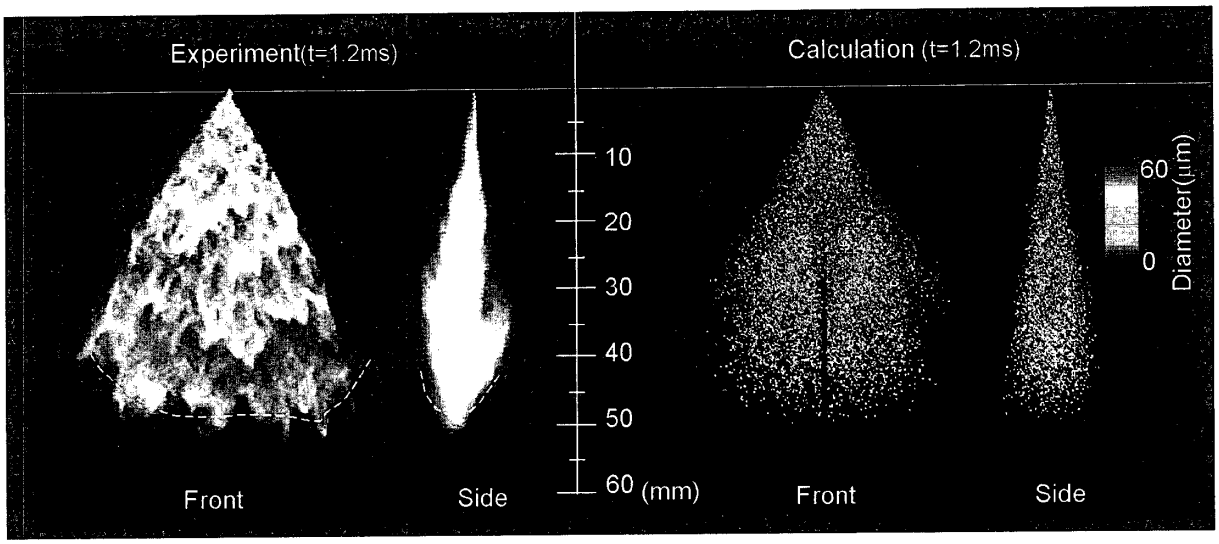


**Fig.21** Comparison of spray image for nozzle B (Pa=280 kPa-abs)

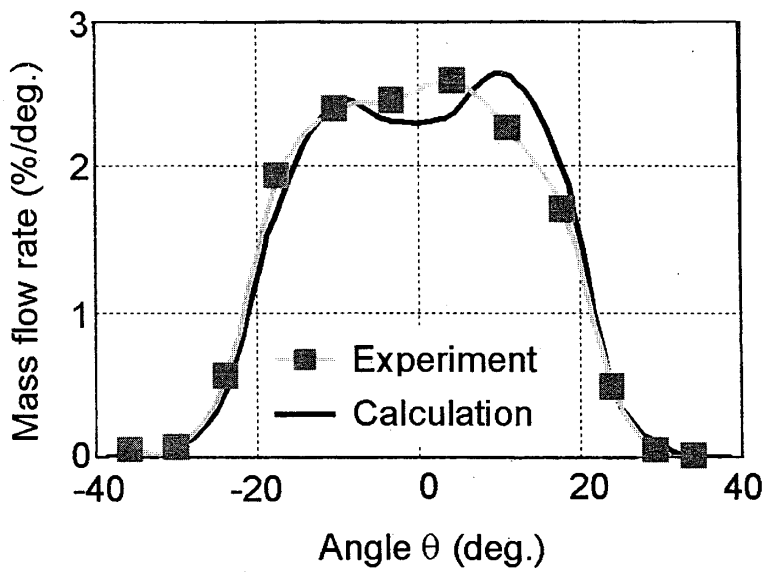


**Fig.22** Mass flow rate distribution for nozzle B

### 4.6 Differences in splay characteristics between nozzle A and B

The cause of the above differences between the two nozzles was investigated. **Figure 23** shows the calculated result of the liquid sheet distribution at the exit of the nozzle B. In the nozzle B, the slit is filled with liquid at the center while the gas phase is observed in the nozzle A. The fuel flow inside the nozzle is investigated in detail so as to clarify the cause of this difference. **Figure 24** shows the flow velocity inside the nozzle. As seen in the cross section 1 of the nozzle A, both sides of the flow along the sac wall collide at the slit entrance, and the flow inside the slit is left-sided. In contrast, the cross section 1 of the nozzle B shows no flow collision, and the flow from the left side goes directly into the slit which is filled with liquid. In cross sections 2 and 3 of both nozzles, A and B, the flow collides at the slit entrance and one-sided in the nozzle hole is seen. As a result, the mass flow rate becomes larger only in the cross section 1 of the nozzle B. This phenomenon must be the cause of the differences in the spray characteristics mentioned above. From this point of view, the above analysis is useful as a tool for efficient nozzle design.

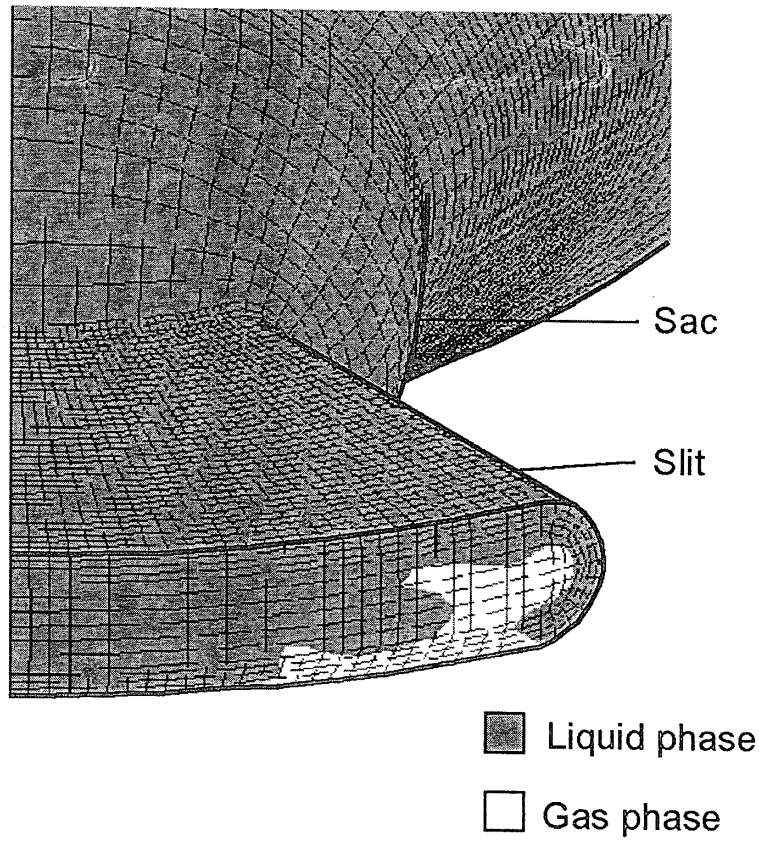


**Fig.23** Nozzle internal flow calculation result for nozzle B

### 4.7 Verification of high temperature condition

Next, we tried to verify the spray characteristics under the high temperature condition. Here, the nozzle A was used, and **Table 4** shows the test conditions. The ambient pressure and the temperature were set at 421 kPa-abs and 479 K, respectively, corresponding to the engine cylinder interior value at the injection. **Figures 25** and **26** show spray images and spray tip penetration, respectively. The calculated spray tip penetration is slightly greater than that of the experiment. The estimated error is about 9% in this verification.

Finally, the spray impinging the wall was investigated in the high pressure and high temperature conditions. The wall temperature was 403 K. The wall-jet model[16] was used as the wall impingement model. The laser-induced fluorescence (LIF) method was used to measure the equivalence ratio in the jet. **Figure 27** shows the LIF system. The laser power and the wavelength used were 50 mJ and 355 nm, respectively. The fuel including 1wt% TMPD (N, N, N', N' tetramethyl-p-phenylene diamine) was used. Fluorescence of wavelength around 400 nm was obtained using the band pass filter and the image intensified camera. **Figure 28** shows the calculated equivalence ratio and the measured one under the high pressure and wall impingement conditions at 5.0 ms after the start of injection. As can be seen in the experiment, the mixture rolled up at 40 - 70 mm horizontal distance from the nozzle. This feature was well simulated by the calculation. The estimated error in the mixture height at the rolled portion was about 24%, while the horizontal tip distance was simulated accurately. **Figure 29** depicts the equivalence ratio 60 mm (horizontally) from the injector and 7 mm (vertically) from the wall. The error in the prediction was about 16% in this verification.

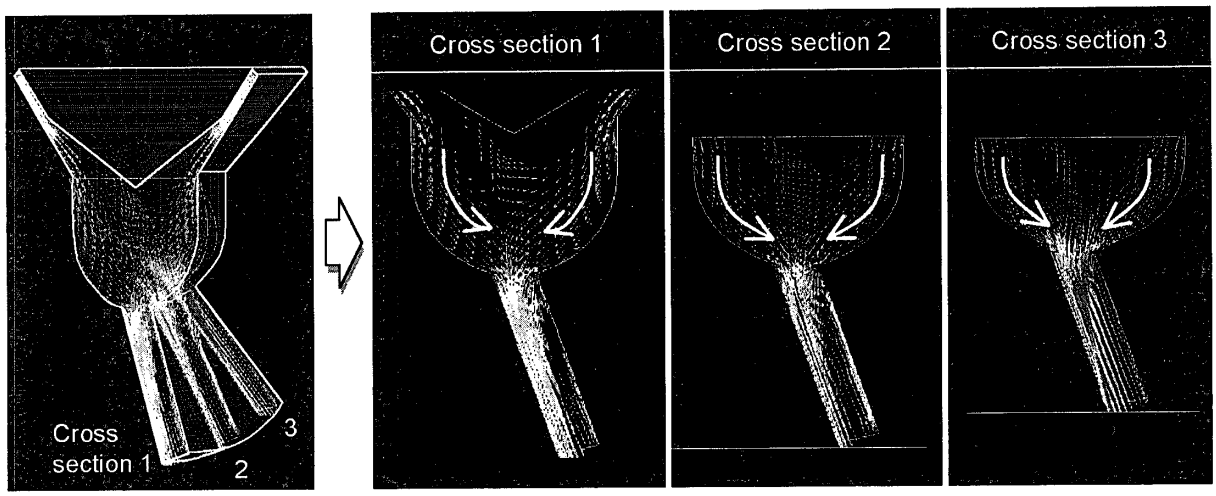


(a) Nozzle A internal flow

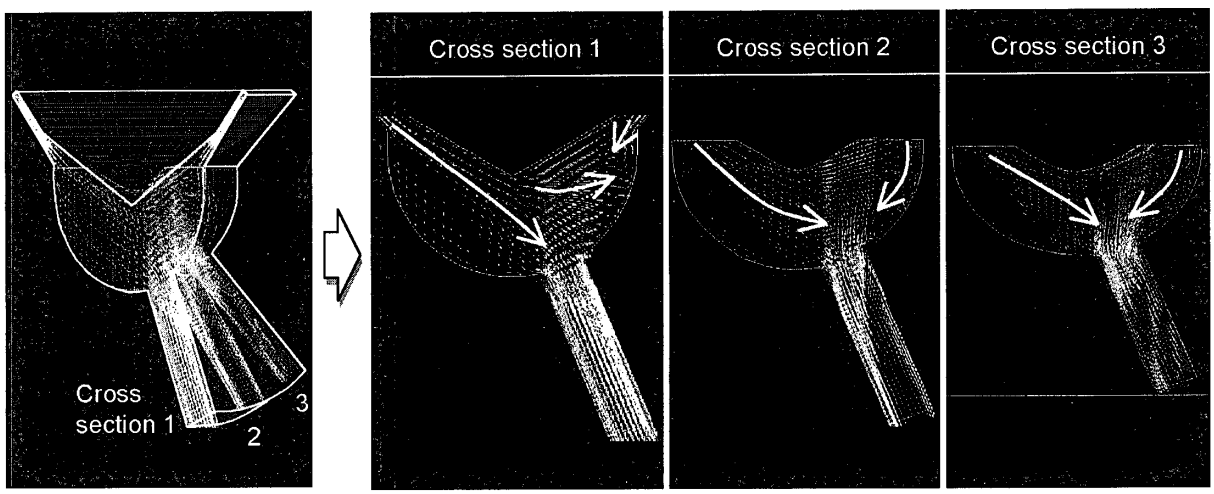


(b) Nozzle B internal flow

**Fig.24** Comparison of nozzle A and B internal flows

**Table 4** Calculation conditions

| Fuel | n-heptan |
|---|---|
| Injection pressure | 11.0MPa-abs |
| Injection pulse | 1.08ms |
| Ambient pressure | 421kPa-abs |
| Ambient temperature | 479K |
| Wall temperature | 403K |

## 5. Conclusions

1. A computational model for the fan spray is proposed. The structure of two-phase flow inside the nozzle is numerically analyzed using the volume of fluid (VOF) method in 3D CFD code based on the nozzle geometry. The results of these analyses are applied to the

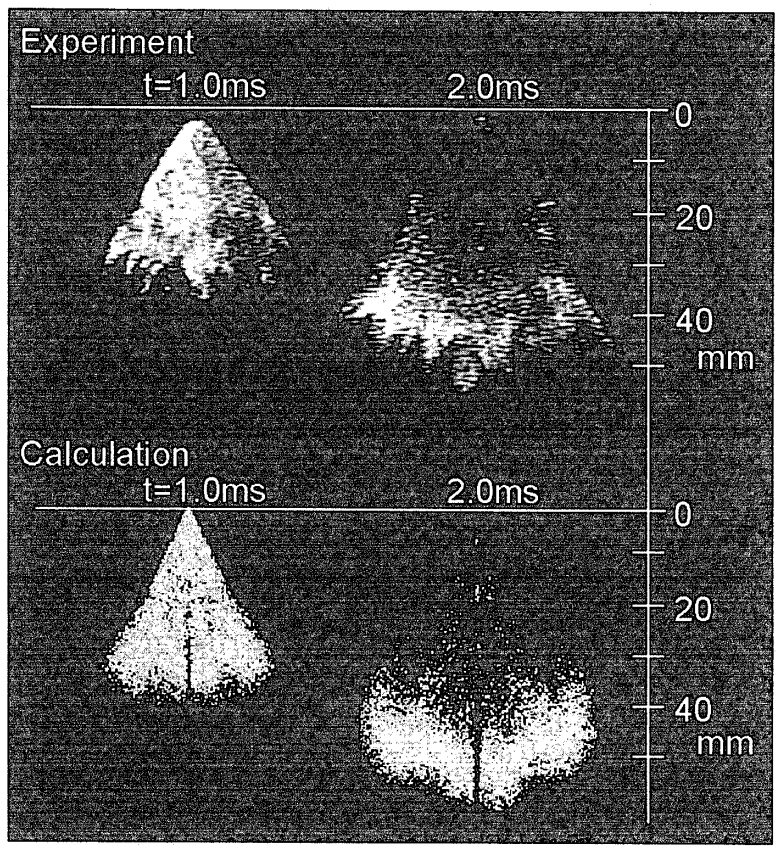


**Fig.25** Spray shape

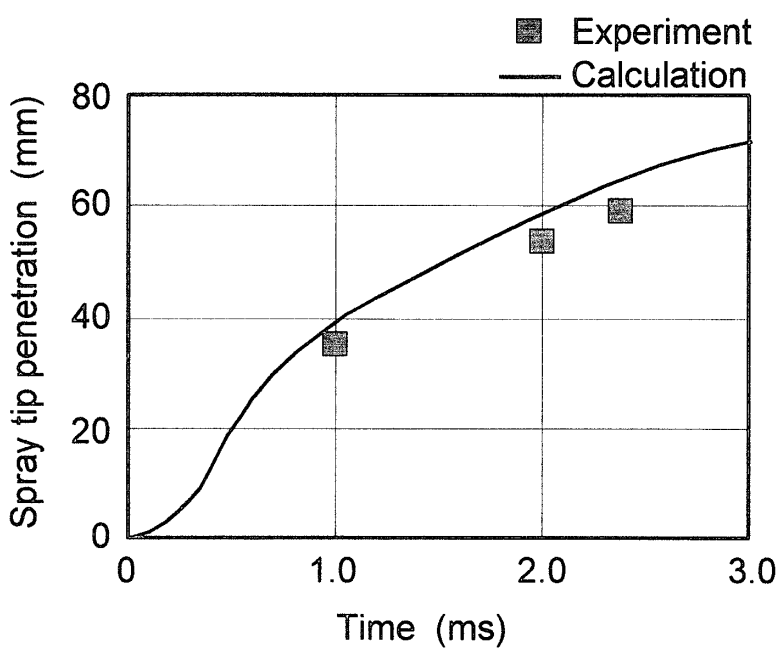


**Fig.26** Spray tip penetration

linear instability theory, to calculate the fuel droplet mean diameter after the primary breakup. These results give the boundary condition at the nozzle exit for the spray simulation without using experimental data and/or empirical laws. The discrete droplet model (DDM) and many sub-models are used for the spray calculation.

2. Various kind of verifications of the spray characteristics were carried out for various pressures and nozzle geometries, such as the spray tip penetration, Sauter Mean Diameter

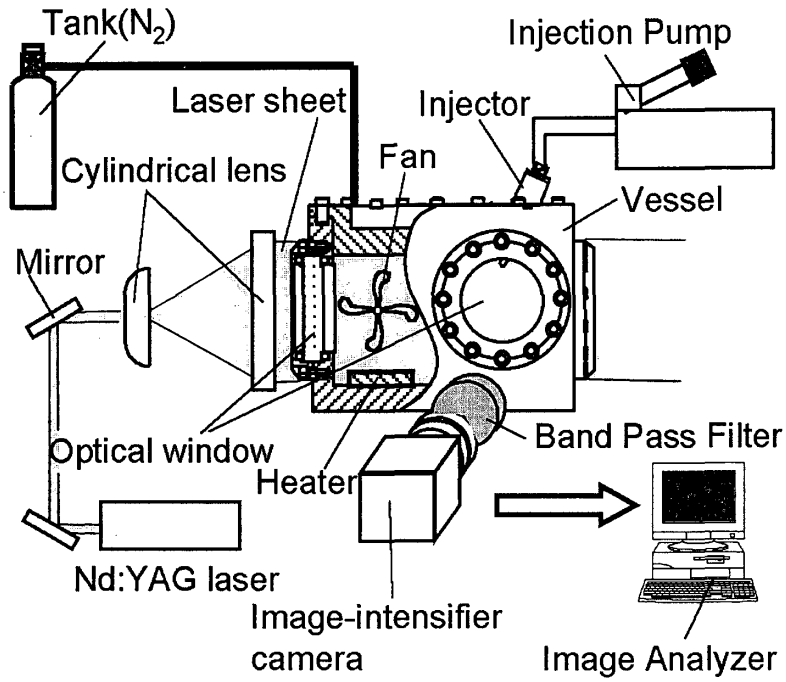


**Fig.27** LIF experimental system

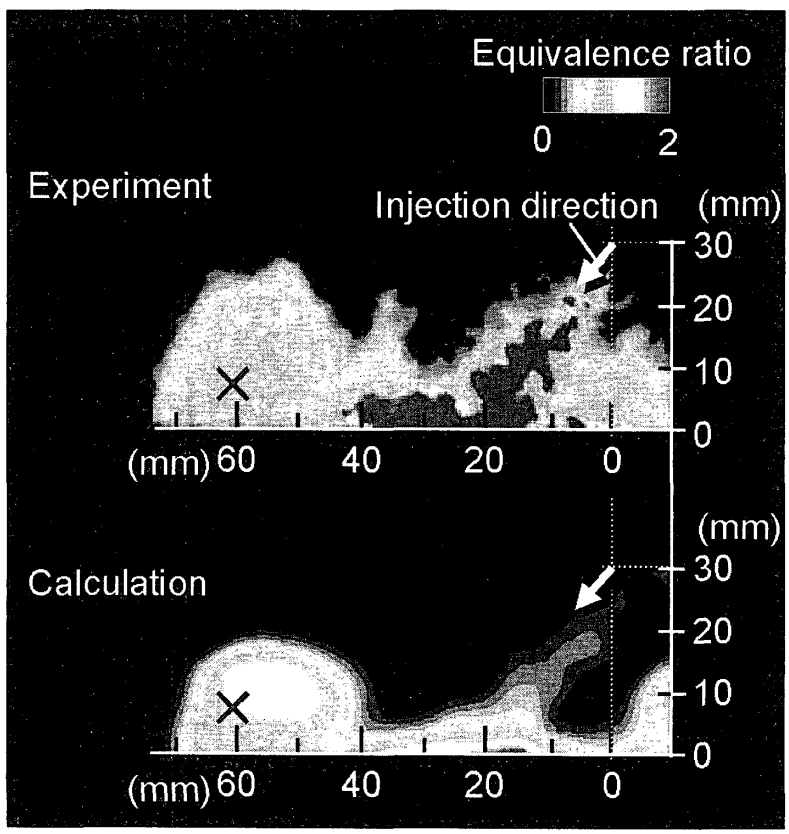


**Fig.28** Fuel vapor distribution of impinging spray

(SMD), the distribution of mass flow rate in the spray, and the equivalence ratio of the mixture.

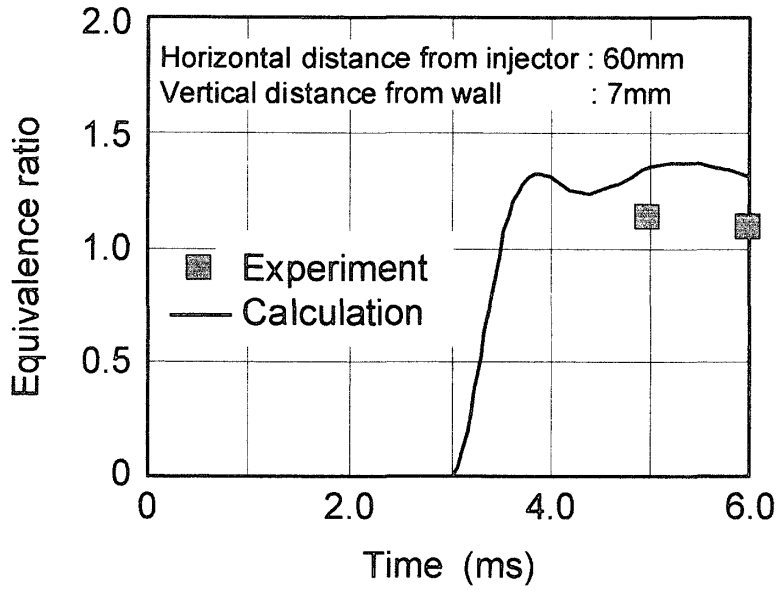


**Fig.29** Equivalence ratio

## References

1) Y. Iwamoto, K. Noma, O. Nakayama, T. Yamauchi, H. Ando, Development of Direct Injection Gasoline Engine, SAE970541, 1997.
2) T. Tomoda, S. Sasaki, D. Sawada, A. Saito, H. Sami, Development of Drect Injection Gasoline Engine - Study of Stratified Mixture Formation, SAE970539, 1997.
3) J. Harada, T. Tomita, H. Mizuno, Z. Mashiki, Y. Ito, Development of Direct Injection Gasoline Engine, SAE970540, 1997.
4) M. Koike, A. Saito, T. Tomoda, Y. Yamamoto, Research and Development of a New Direct Injection Gasoline Engine, SAE2000-01-0530, 2000.
5) M. Kanda, T. Baika, S. Kato, M. Iwamuro, M. Koike, A. Saito, Application of a New Combustion Concept to Direct Injection Gasoline Engine, SAE2000-01-0531, 2000.
6) S. Ueda, Y. Mori, E. Iwanari, Y. Oguma, Y. Minoura, Development of a New Injector in Gasoline Direct Injection System, SAE2000-01-1046, 2000.
7) J. K. Dukowicz, A Particle-Fluid Numerical Model for Liquid Sprays, J. Comp. Physics, vol.35, pp.229-253, 1980.
8) W. M. Ren, J. F. Nally Jr., Computations of Hollow-Cone Sprays from a Pressure-Swirl Injector, SAE982610, 1998.
9) M. Xu, L. E. Markle, CFD-Aided Development of Spray for an Outwardly Opening Direct Injection Gasoline Injector, SAE980493, 1998.
10) C. Arcoumanis, M. Gavaises, B. Argueyrolles, F. Galzin, Modeling of Pressure-Swirl Atomization for GDI Engines, SAE1999-01-0500, 1999.
11) A. H. Lefebvre, Atomization and Sprays, Combustion: An International Series, Hemisphere, 1989.
12) R. P. Fraser, P. Eisenklam, N. Dombrowski, D. Hasson, Drop Formation from Rapidly Moving Liquid Sheets, A. I. Ch. E. Journal, vol.8, no.5, pp.672-680, 1962.
13) C. W. Hirt, B. D. Nichols, Volume of Fluid (VOF) Method for the Dynamics of Free Boundaries, Journal of Comp. Physics, no.1, 39, pp.201-225, 1981.
14) R. D. Reitz, Modeling Atomization Processes in High-Pressure Vaporizing Sprays, Atomization and Spray Technology, vol.3, pp.309-337, 1987.

15) A. B. Liu et al., Modeling the Effects of Drop Drag and Breakup on Fuel Sprays, SAE930072, 1993.
16) J. D. Naber, R. D. Reitz, Modeling Engine Spray-Wall Impingement, SAE880107, 1988.
17) K. Takeda, T. Sugimoto, T. Tuchiya, M. Ogawa, S. Ueda, K. Yoneshige, Slit Nozzle Injector for A New Concept of Direct Injection SI Gasoline Engine, SAE2000-01-1902, 2000.
18) A. Okamoto, T. Sato, N. Shirabe, Y. Anezaki, Developmemt of Fan Spray Simulation for Gasoline Direct Injection Engines, SAE2001-01-0962.